Bull Volcanol (2008) 70:655–673
DOI 10.1007/s00445-007-0160-3

RESEARCH ARTICLE

The 2005 eruption of Sierra Negra volcano, Galápagos, Ecuador

Dennis J. Geist · Karen S. Harpp · Terry R. Naumann · Michael Poland · William W. Chadwick · Minard Hall · Erika Rader

Received: 15 September 2006 / Accepted: 16 May 2007 / Published online: 31 July 2007

Abstract Sierra Negra volcano began erupting on 22 October 2005, after a repose of 26 years. A plume of ash and steam more than 13 km high accompanied the initial phase of the eruption and was quickly followed by a ~2-km-long curtain of lava fountains. The eruptive fissure opened inside the north rim of the caldera, on the opposite side of the caldera from an active fault system that experienced an m_b 4.6 earthquake and ~84 cm of uplift on 16 April 2005. The main products of the eruption were an `a`a flow that ponded in the caldera and clastigenic lavas that flowed down the north flank. The `a`a flow grew in an unusual way. Once it had established most of its aerial extent, the interior of the flow was fed via a perched lava pond, causing inflation of the `a`a. This pressurized fluid interior then fed pahoehoe breakouts along the margins of the flow, many of which were subsequently overridden by `a`a, as the crust slowly spread from the center of the pond and tumbled over the pahoehoe. The curtain of lava fountains coalesced with time, and by day 4, only one vent was erupting. The effusion rate slowed from day 7 until the eruption's end two days later on 30 October. Although the caldera floor had inflated by ~5 m since 1992, and the rate of inflation had accelerated since 2003, there was no transient deformation in the hours or days before the eruption. During the 8 days of the eruption, GPS and InSAR data show that the caldera floor deflated ~5 m, and the volcano contracted horizontally ~6 m. The total eruptive volume is estimated as being ~150×10^6 m^3. The opening-phase tephra is more evolved than the eruptive products that followed. The compositional variation of tephra and lava sampled over the course of the eruption is attributed to eruption from a zoned sill that lies 2.1 km beneath the caldera floor.

Keywords Caldera · Basalt · Galápagos · Tephra · Lava flow emplacement · Volcano deformation · Magma chamber processes

Editorial responsibility: J Stix

D. J. Geist (✉)
Department of Geological Sciences, University of Idaho 3022, Moscow, ID 83844, USA
e-mail: dgeist@uidaho.edu

K. S. Harpp · E. Rader
Geology Department, Colgate University, Hamilton, NY 13348, USA

K. S. Harpp
e-mail: kharpp@mail.colgate.edu

T. R. Naumann
Geology Department, University of Alaska, Anchorage, AK, USA
e-mail: aftrn@uaa.alaska.edu

M. Poland
USGS-HVO, P.O. Box 51, Hawai'i National Park, HI, USA
e-mail: mpoland@usgs.gov

W. W. Chadwick
Hatfield Marine Science Center, Oregon State University, Newport, OR 97365, USA
e-mail: William.W.Chadwick@noaa.gov

M. Hall
Instituto Geofisico, Escuela Politecnica Nacional, Quito 17-01-2759, Ecuador

Introduction

There is an eruption every few years in the Galápagos Archipelago, but only recently have the eruptions been

observed and monitored by volcanologists equipped with instrumental and petrological tools (e.g., Allan and Simkin 2000; Teasdale et al. 2005). Sierra Negra volcano began its first eruption in 26 years on 22 October 2005. The eruption provided new opportunities for the study of active volcanism because the volcano's geologic history is well known (Reynolds et al. 1995; Jonsson et al. 2005); geodetic studies in the 13 years prior to the eruption have provided constraints on recent magmatism and tectonism (Amelung et al. 2000; Geist et al. 2006; Chadwick et al. 2006), and modern communications and good fortune enabled direct observations during much of the eruption.

This work takes a multidisciplinary approach to studying the 2005 eruption of Sierra Negra. First, visual and photographic observations are described and applied to recent models of vent processes and lava flow emplacement. Second, results from continuous Global Positioning System (GPS) and satellite radar interferometry (InSAR) measurements are used to constrain the history of magma discharge from the shallow chamber as well as pre-eruptive deformation phenomena. Third, results from geochemical and petrologic studies of a time-series collection of lava and tephra samples are used to assess pre- and syn-eruptive differentiation and crystallization processes.

Geologic background

Sierra Negra is the most voluminous and one of the most active volcanoes in the Galápagos Archipelago (Fig. 1; Simkin and Siebert 1994). The archipelago is related to a hotspot that lies 100–300 km south of the Galápagos Spreading Center. Because the Nazca plate is moving eastward, historical volcanic activity has been concentrated in the western part of the archipelago.

The geologic history of Sierra Negra is described by Reynolds et al. (1995). The oldest known rocks on the volcano crop out on the southern and eastern flanks and are <7,000 years old (Reynolds et al. 1995). The most recent activity has been within the caldera and from circumferential vents near the northern caldera rim. The long-term eruptive rate of Sierra Negra is estimated to be ~1×10^6 m^3/year (Reynolds et al. 1995).

Sierra Negra's caldera has plan dimensions of 9×7 km, with the major axis oriented NE–SW. The caldera is structurally complex, with a prominent sinuous ridge that is subparallel to the caldera wall (Fig. 2). This ridge is an upthrust part of the caldera floor, and in places it has been uplifted higher than the caldera rim. The fault that bounds the outward margins of this ridge remains active, with documented earthquakes in 1998 (Amelung et al. 2000), 16 April 2005 (Chadwick et al. 2006), and just before the 2005 eruption (Yun et al. 2006b). Onlapping lava flows form unconformities on the ridge's inward-facing slopes, indicating a prolonged history of uplift interspersed with caldera-ponded eruptions.

Measurements by GPS and InSAR indicate that the caldera floor has a dynamic record of inflation and deflation since at least 1992 with about 5 m of total uplift preceding

Fig. 1 Shaded relief map of the central Galápagos Archipelago, showing the location of Sierra Negra volcano. *Box* outlines the caldera of Sierra Negra. *Inset* shows the location of the Galápagos Archipelago on a regional scale. Figure courtesy of Sang-Ho Yun

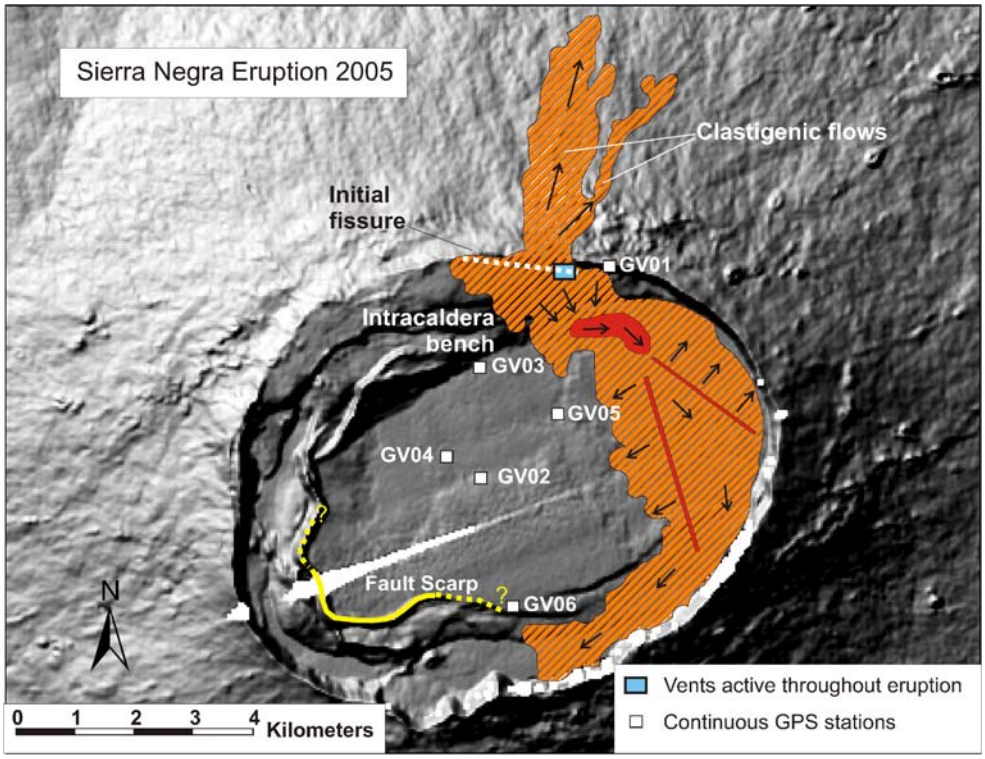

Fig. 2 Shaded relief map of the summit area of Sierra Negra volcano. The 2005 lava flow is shown in *orange*, with *arrows* indicating flow directions. *Red lines* indicate clefts from which the lava flow spread during inflation. *Red region* is location of the perched lava pond that fed the interior of the flow after its initial emplacement

the 2005 eruption (Amelung et al. 2000; Geist et al. 2006; Chadwick et al. 2006). The pattern of inflation is domal over the long-term but is punctuated by trapdoor faulting events along the sinuous-ridge faults (Amelung et al. 2000; Jonsson et al. 2005; Yun et al. 2006a; Chadwick et al. 2006). Between 1992 and early 1998, the caldera floor bulged elastically nearly 2 m (Amelung et al. 2000), culminating in a trapdoor faulting event along the southern extent of the caldera floor fault system (Fig. 2). Inflation renewed after the faulting event but decelerated sometime in 2000–2001, when the caldera floor began deflating (Geist et al. 2006). Models of the deformation from 1992 to 2000 (Amelung et al. 2000; Yun et al. 2006a) and 2000 to 2002 (Geist et al. 2006) are both consistent with a 3×5 km flat-topped chamber or sill centered ~2.1 km beneath the caldera floor.

Sierra Negra has had ten recorded historical eruptions (Simkin and Siebert 1994). Repose times have ranged from 4 to 37 years, with an average of 15 years. The most recent eruption before 2005 was in 1979, which was an unusually prolonged and voluminous event, with an estimated output of nearly 9×10^8 m^3 of lava (Reynolds et al. 1995). Eruptive fissures at Sierra Negra are circumferentially disposed about the caldera near the summit, and radial on the flanks of the volcano (Reynolds et al. 1995). All described historical eruptions prior to 2005 have been from circumferential fissures north of the caldera floor.

Sierra Negra has an active hydrothermal system (Simkin and Siebert 1994; Goff et al. 2000). The most vigorous vents are at the western end of the sinuous ridge. New fumaroles became active in early 2005 along the southeastern part of the sinuous ridge, about 1 km east of GPS station GV06 (Fig. 2; Patricio Ramón, personal communication, 2005). Until the 2005 eruption, the 1979 vents also were steaming, although with decreasing vigor over the past 20 years.

Sierra Negra's lavas are tholeiitic basalts, with a small compositional range (Reynolds and Geist 1995). Most lavas are sparsely porphyritic, typically with <5% plagioclase phenocrysts. Most of the compositional variation is attributed to fractional crystallization of plagioclase + augite + olivine, at pressures ranging from 100 to 300 MPa.

Eruption chronology

Field observations

Sierra Negra volcano began erupting at approximately 1730 local time (LT) on Saturday, 22 October 2005 (2330 UTC). To the best of our knowledge, there were no direct observations of the fissure opening in the first minutes of the eruption. A M_w 5.5 earthquake preceded the eruption at 1434 LT (2034 UTC; National Earthquake Information Center; http://neic.usgs.gov). The precise location of this earthquake was not measured. In June 2006, we discovered a fresh vertical fault scarp on the southern and western parts of the sinuous ridge (Fig. 2), which had ~150 cm of dip-slip displacement, with the northeastern block up. Modeling of

coeruptive InSAR images is consistent with major displacement centered on the western part of the sinuous ridge (Yun et al. 2006b).

Eyewitness reports indicate that the initial volcanic plume was >10 km in height, and our measurements from photos taken in the first hour of the eruption (Fig. 3a) yield estimates of 13–14 km. Hall observed the plume from the highlands of Santa Cruz island at 2030 LT and estimates that it was 13–15 km high. The plume was carried to the west, depositing a tephra blanket across the northern and western flanks of the volcano. Photos taken from Alcedo volcano, approximately 40 km northeast of the Sierra Negra summit, reveal that a fissure had opened along the northern caldera rim by 1800 LT. Approximately 40 min later, the fissure had extended to the east, tripling in length. Activity appeared to be concentrated at the two ends of the fissure, most strongly along the western third. Beginning ~2030 LT, activity along the western segment of the fissure increased in intensity, forming a chain of discrete lava fountains. Within the next 45 min, a clastigenic flow supplied by the lava fountains rooted inside the caldera had established at least four distinct channels down the north flank of the volcano.

At 0700 LT on Sunday, 23 October (day 2), the plume was weaker than on the first day of the eruption, extending only several kilometers high with a diffuse source along the entire ~2 km length of the fissure. The caldera was visited at 0745 LT by Galápagos National Park and Darwin Research Station officials. By this time, the most vigorous activity along the fissure had switched to the eastern end, where two major vents were continuously producing fountains up to 300 m high, and three smaller vents were active less than 200 m to their east. Small areas of incandescence remained visible on the western end of the fissure, and a single lava fountain there threw spatter to about 20 m, but the amount of lava being emitted from the western vents was insignificant. Spatter from the two large eastern vents continued to coalesce into a clastigenic flow that extended ~5 km down the north flank.

All of the vents were located inside the caldera rim throughout the eruption, and the lava on the north flank originated from coalesced pyroclasts erupted from the intracaldera lava fountains. Most of the lava emplaced in the caldera was erupted from 5 vents, which supplied a ~2 km-wide anastamosing flow field that cascaded down intracaldera benches to the caldera floor. Lava in the channels was estimated to be flowing at ~15 m s^{-1} and formed standing waves >5 m high. The intracaldera flow ponded to form a ~2 km wide `a`a field that extended to the southeast caldera wall approximately 4 km south of the vent, banked against it, and curved in a 1 km-wide lobe that eventually reached about 1.5 km west (Fig. 2). The flow front advanced westward in the moat between the caldera wall and the southernmost scarps forming the sinuous ridge, while closer to the vents, the flow spread more slowly laterally to the west along most of its length. Vigorous fumaroles on the caldera wall about 200 m east of the easternmost vent may mark the extension of the fissure-feeding dike in that direction. Subsequent field observations coupled with photographic evidence suggest that these fumaroles may have also been the site of small fire fountains, forming short spatter-fed flows, which extended into the caldera sometime during the first 3 days of the eruption.

Lapilli and Pele's hair erupted in the initial explosive phase of the eruption were deposited along the caldera rim up to 4 km south of the vents and >5 km to the west. The latter deposits are in line with the higher altitude prevailing winds according to early satellite images. Within 500 m of the vents, most of the pyroclastic material is scoriaceous lapilli >1 cm in diameter.

On the third day of the eruption (24 October), activity focused to two or three vents, and the eruptive intensity decreased (Fig. 3b). Instead of a widespread flow field across the intracaldera benches, lava was organized into five distinct braided channels. These cascaded down the benches to feed a >1-km-wide lava pool on the northern caldera floor, which in turn supplied the intracaldera `a`a field. On 25 or 26 October (day 4 or 5) the easternmost vent shut down, leaving only one active vent near the eastern terminus of the fissures. Witnesses reported that at approximately 0830 on 27 October, the major eastern vent re-opened, without any loss of intensity at the western vent. Three of the coauthors (KH, DG, and TN) arrived at the eruption on the afternoon of 27 October.

Lava fountaining on the evening of 27 October (day 6) produced spatter clasts up to 30 cm in diameter, which were being deposited to the northeast (downwind) onto the outer flank of the volcano, within 100 m of the vent. We estimate that the highest fountain, a directed, collimated jet from the western vent, extended to 50 m. The fountain at the eastern vent was wider and reached only ~30 m in height. Gases were emitted as nearly continuous jets from all vents, and the lava fountaining was steady. During fountaining, the majority of the fragments were recycled back into the vents, some by falling directly back into the craters and others by avalanching of still-incandescent slabs down the inner crater walls. The spatter accumulated quickly enough on the outer flanks (primarily from the stronger western lava fountain) to coalesce and feed the easternmost clastigenic `a`a flow, which remained incandescent over 1 km down the north flank of the volcano (Fig. 2).

By the evening of 27 October, three braided channels supplied the intracaldera lava flow, each 10–20 m wide. The channels crossed the northern caldera bench, two originating from the western vent and one from the eastern

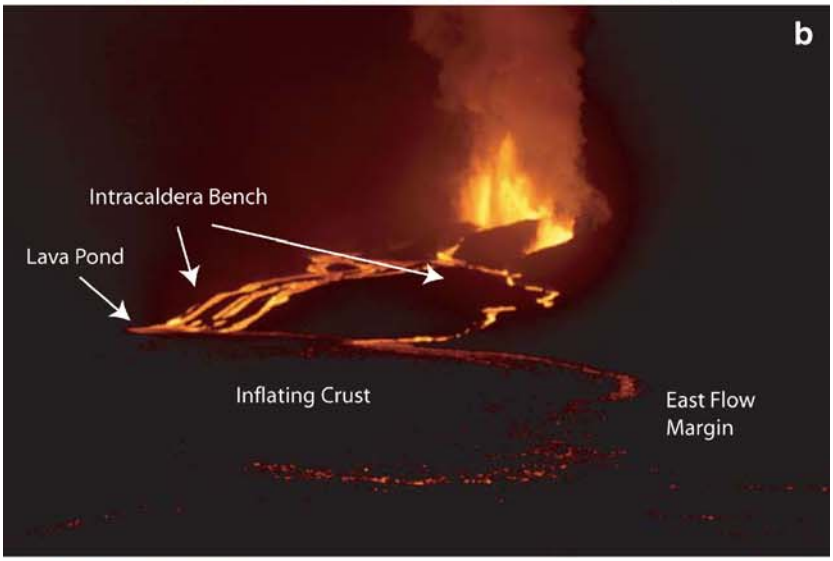

Fig. 3 **a** Photograph of the initial plume (by Askel Voigt) taken from about 100 km north of Sierra Negra at 1734 local time on 22 October 2004. The plume is estimated to be 13–14 km high. **b** Photograph of the eruption on 24 October taken by Greg Estes from the southeast. By this time, the original ~2 km fissure was erupting only from its eastern margin. Four lava channels can be seen spilling over the intracaldera bench and feeding the caldera floor flow, whose eastern margin is incandescent and in the foreground. **c** The waning stage of the eruption, when it changed to a pulsating Strombolian style, taken from about 100 m east of the last open vent. The single active open channel can be seen in the background

vent. The estimated velocity of lava in the channels exceeded 10 m s^{-1}, sufficient to set up standing waves in the lava as it rounded corners and reversals at small drops in elevation. Periodic increases in the flux of lava, often caused by avalanches of accumulated spatter back into the vents, would cause extensive channel overflows, mostly as pahoehoe.

The intracaldera lava flow did not lengthen significantly beyond the first two days of the eruption; instead, from the second day forward, the flow enlarged by slowly spreading laterally, mostly westward up the east-sloping caldera floor. Lava was delivered to the western margin through the interior of the flow, while the surface crust inflated and spread more slowly (only several m/day). The lateral growth of the flow occurred by extrusion of pahoehoe lobes from the `a`a front. The pahoehoe front was then overridden by `a`a as the crust spread, presumably sliding downhill owing to inflation and elevation of the flow's center. The spreading tore two ~3 km long clefts in the flow top, as well as multiple 10–30 m-long cracks, and smooth lava welled up to fill them. A contributing factor to spreading on the west margin may have been the several-meter deflation of the center of the caldera over the course of the eruption, as measured by GPS and discussed below. Post-eruption inspection of the southwestern terminus of the lava flow (9 km from the vent) revealed that toothpaste lava also oozed out of the flow top during this episode of the eruption (Rader et al. 2006).

The flux of lava, spatter, and gas emitted by the two vents increased notably beginning around midday on the seventh day of the eruption, 28 October. Several tremors that coincided with the change in activity were felt within ~300 m of the vents. By sunset, the bases of both fountains had widened by several meters with no decrease in fountain height. The previously braided lava flows on the bench focused into two main channels over the course of the afternoon. On the basis of velocity measurements and post-eruption inspection of the channels, we estimate that the eruptive flux at this time was ~100 m^3 s^{-1}.

During the early morning hours of 29 October (day 8), the western vent stopped erupting, producing only gas. The eastern vent continued to fountain (Fig. 3c), but instead of a steady jet, the fountain pulsated between 20 and 50 m in height every 1–5 s. Over the course of the day, the vigor of the fountaining steadily decreased, and a lava lake became visible in the eastern crater for the first time. By this time, the level of the lava in the channel fed by the eastern vent had dropped by about 50% relative to the previous day. That evening, the velocity of lava in the channel was measured to be 4 m s^{-1}. Consequently, we estimate that the eruptive flux had decreased to ~25% of the previous day's rate (or ~25 m^3 s^{-1}).

The eruption terminated between 0200 and 0400 LT on the ninth day of the eruption, 30 October. Strong plumes of gas continued to be emitted from the vents, particularly the western one. The final area of the intra-caldera lava flow is 14.2 km^2 and that of the extra-caldera clastigenic lava flows 4.1 km^2. The distal flow front of the intracaldera flow 9 km from the vent is estimated to be ~10 m thick. If this is the average thickness of the entire intracaldera flow, then the bulk volume of this flow is 1.5×10^8 m^3.

The eruption had little effect on the wildlife, a particular concern in the Galápagos National Park, mainly because the tephra and lavas covered areas comprising young poorly vegetated deposits. The population of rare giant tortoises from Sierra Negra, *Geochelone Guntheri*, was unaffected. The lava flow ignited wildfires that caused much of the vegetated caldera wall and upper southwestern slopes to burn for over a month after the cessation of the eruption.

In February 2006, several fumaroles continued to vent from the main body of the lava flow on the caldera floor, and substantial gas was being emitted from the western vent. White mineral deposits decorated the flow where now-extinct fumaroles had vented, and yellow sulfur deposits were visible west of the main vents and at some locations on the caldera floor flow. Meter-scale cracks and slumping of the eastern edge of the `a`a flow had occurred along the caldera wall, likely the result of deflation of the intracaldera flow as it cooled.

As of June 2006, the western vent was still producing gas but at a decreased rate relative to February, 2006. The caldera floor fumaroles continued to degas at a vigorous rate, producing plumes several tens of meters in height and varying in intensity every few minutes. Smaller fumaroles were observed emanating from the rootless flows on the north flank. The clastigenic flows that were coated in tephra on the flank and the pool at the base of the caldera bench remained hot enough to emit visible heat shimmers.

Satellite observations

A thermal anomaly was detected at 2345 UTC on 22 October by the GOES satellite system http://goes.higp.hawaii.edu/); the previous image had been collected at 2315 UTC and showed no anomaly, confirming eyewitness reports of the initiation of the eruption. Hotspots were visible in the GOES images around the vent and within the caldera over the course of the entire eruption, and the cooling intracaldera lava flow was observable through 16 November 2005. The eruptive plume was also detected in NASA MODIS data http://visibleearth.nasa.gov/). An image from 23 October shows a dense cloud approximately 40 km in diameter centered over the volcano and a more diffuse haze extending for at least 200 km to the WNW. On 25 October the plume margins were much sharper than before and extended for over 400 km to the west of the volcano. Images from 30 October reveal no distinct plume,

but instead a low-level volcanic haze that spread to the west covering an area >400 km across.

Measurements by the Ozone Monitoring Instrument spanning 23 October through 1 November showed a robust SO_2 plume over the course of the eruption http://www.knmi.nl/omi/publ-en/news/archive/2005/index_en.html). Levels of SO_2 >1.5 Dobson units were present over an area of ~3,300×1,100 km, extending west of the volcano, with more diffuse concentrations reaching twice this distance. The maximum concentration was >3 Dobson units.

Deformation observations

In 2002, a continuous GPS network was installed on Sierra Negra (Chadwick et al. 2006), which recorded minor deflation until April 2003, when inflation began. The inflation accelerated over the next 2 years until on 16 April 2005, a fault on the southern part of the sinuous ridge ruptured, causing a m_b 4.6 earthquake and raising the southern part of the caldera floor 84 cm in a southern-dipping trapdoor geometry. Inflation about the center of the caldera was not affected by the earthquake and continued to accelerate until it reached a rate of about 2.5 m/year in the months preceding the 2005 eruption (Chadwick et al. 2006). The total uplift of the center of the caldera floor between April 2003 and the start of the 2005 eruption was 2.2 m. The ~5 m of uplift between 1992 and 2005 is the largest recorded on a basaltic volcano (Chadwick et al. 2006) and was caused by the intrusion of magma into a reservoir at ~2.1 km depth.

Despite the long-term pattern of uplift of the caldera floor, continuous GPS data yielded no immediate precursor to the eruption; the positions of stations within the caldera on the days before the 22 October eruption lie precisely on the trends from the previous weeks (Fig. 4). However, no GPS data are available for the last 16 h leading up to the eruption, because a hardware failure occurred and the network was not restored until 24 October. Also, no dual-frequency receiver had been operating in the region since early September, and the only sites working during the eruption were on the caldera floor. This conspiracy of failures resulted in two lost opportunities. First, deformation related to the precursory M_w 5.5 earthquake and the initiation of the eruption was not recorded. Second, the position of the four-station single-frequency network relative to a fixed point is uncertain. Thus, the GPS data during the eruption were processed as baselines connecting to station GV03 (Fig. 2).

During the eruption, the center of the caldera floor (GV04) dropped by about 2.4 m relative to GV03 (Fig. 5a), and the N–S diameter of the caldera floor (GV03–GV06) contracted horizontally by >6 m (Fig. 5b). Most of the deflation occurred during the first two days of the eruption. The deflation rate then decreased until the end of the eruption on 30 October, when inflation resumed immediately.

Co-eruptive surface displacements were also measured by satellite radar interferometry (InSAR). The European Space Agency ENVISAT satellite acquired SAR data from multiple look angles over Sierra Negra both before and after the eruption. We used these data to construct several 35-day co-eruption interferograms following the procedures of Chadwick et al. (2006) and using the merged SRTM-TOPSAR data of Yun et al. (2005) for topographic corrections. The most coherent of these is from track 61, beam mode 2, and spans

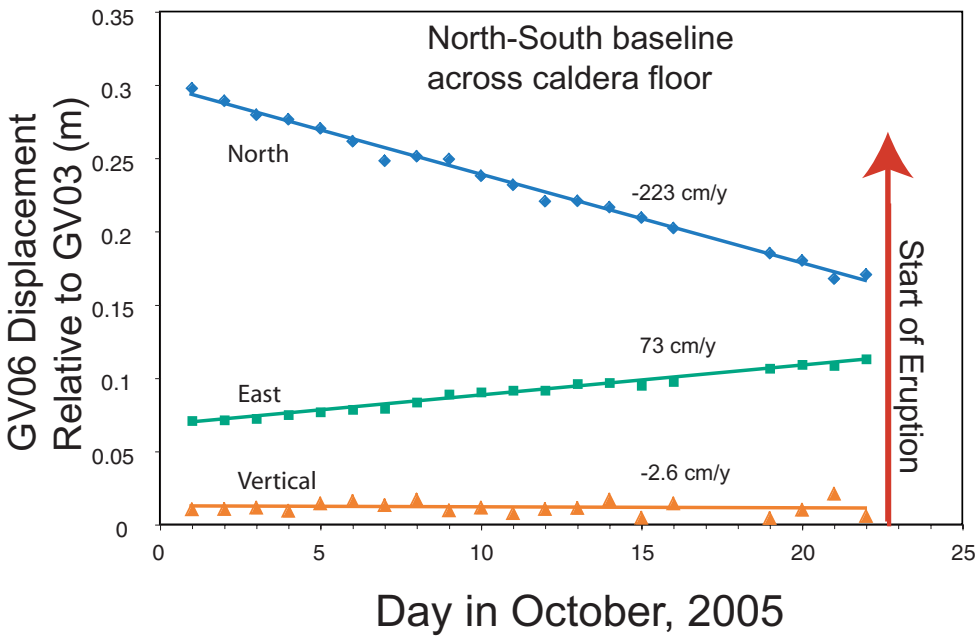

Fig. 4 Position changes of a roughly N–S baseline across the caldera floor, from GV03 to GV06 (Fig. 2). Horizontal extension of this baseline is the most sensitive one in the network to precursory deformation. No inflection in the longer-term motions is apparent, suggesting that any deformation directly related to the intrusion of the fissure-feeding dike did not occur until immediately before the eruption

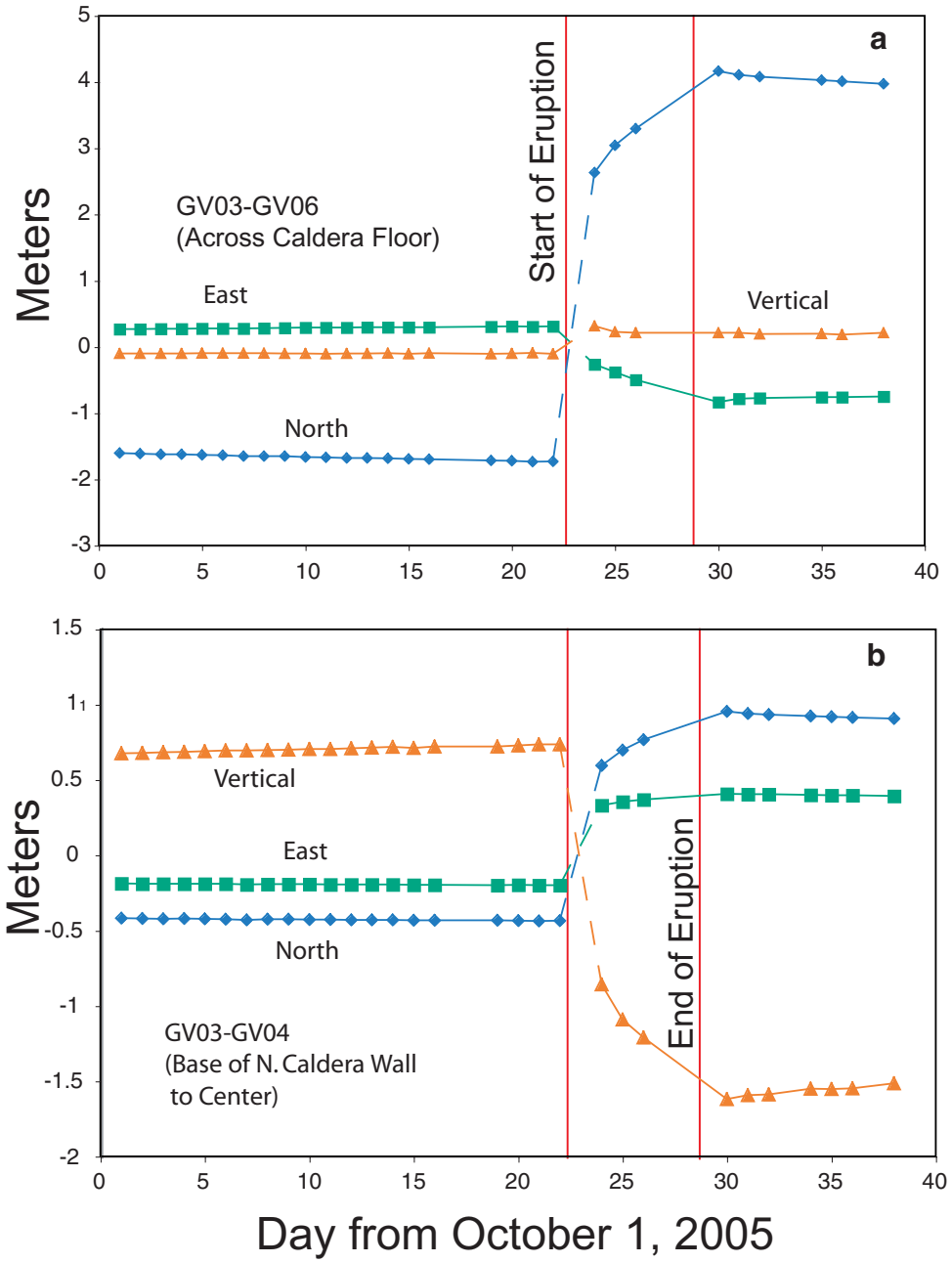

Fig. 5 a, b Position changes across two baselines, expressed in three directional components and spanning the duration of the eruption; note the different scale compared to Fig. 4, which encompasses the pre-eruption deformation. The first baseline is between the north and south margins of the caldera floor (GV03–GV06; Fig. 2) and the other from the northern caldera floor to near the caldera center (GV03–GV04). Subsidence and contraction rates decelerate over the course of the eruption. Inflation began within a day after the end of the eruption on October 30

24 September to 29 October 2005 (Fig. 6a). The time spanned by this interferogram therefore includes about 1 month of pre-eruption deformation, which, based on GPS measurements, probably amounts to 20 cm of uplift at the center of the caldera, and little motion outside the caldera.

Line-of-sight (LOS) deformation in all co-eruption interferograms is dominated by deflation that extends well outside the caldera boundaries. This is a significant departure from previous results, which have noted only minor deformation outside the confines of the caldera (Amelung et al. 2000; Geist et al. 2006; Yun et al. 2006a, b; Chadwick et al. 2006). Unfortunately, the caldera floor is almost completely incoherent in all co-eruption interferograms, attributable to the several-meter co-eruption displacements demonstrated by GPS measurements. Although this incoherence obscures the large signal associated with the eruption, it also means that nearly all the LOS deformation in the co-eruption interferograms is related to the eruption, because pre-eruption deformation was not significant beyond the caldera.

The maximum line-of-sight lengthening (deflation) in the most coherent interferogram (Fig. 6a) is about 30 cm and occurs on the north edge of the caldera. There is also a region of line-of-sight shortening of about 5 cm centered 1 km east of the east caldera rim, which is probably a result of a combination of the non-vertical look angle and the co-

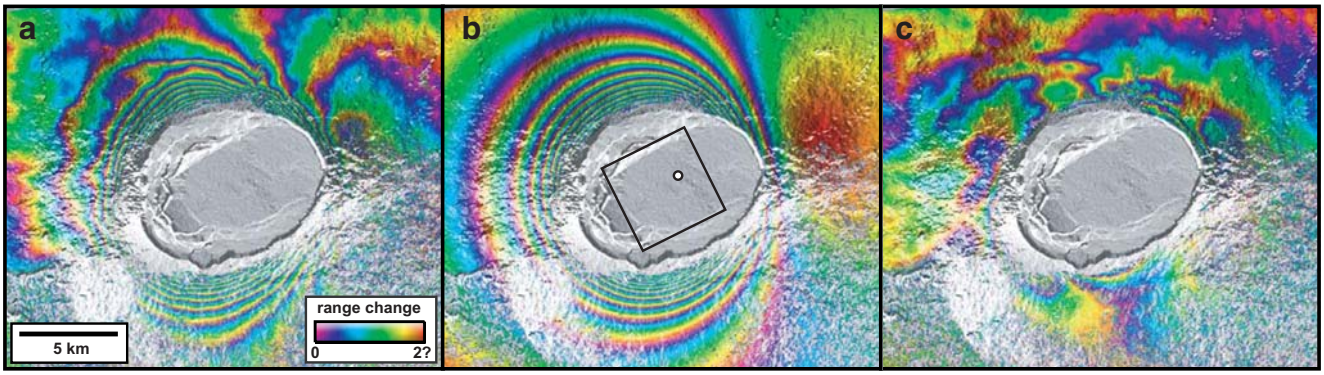

Fig. 6 **a** ENVISAT beam mode 2, track 61 interferogram spanning 24 September to 29 October 2005 showing broad subsidence of Sierra Negra volcano. The caldera is incoherent due to modification by lava flows and high deformation gradients. **b** Predicted range change from a model consisting of a uniform opening sill (*black box*) and a point source of volume loss (*white circle*), both at 2 km depth. **c** Residual range change. Color and distance scales are the same in all three parts

eruption displacements, however, and not an indication that a center of uplift exists east of the caldera.

Petrology and geochemistry

Tephra samples were collected as they fell on four days of the eruption, 23 October and 27–29 October (Table 1). Additional samples (SN05-02 and SN05-A) gathered 4 km from the fissure almost certainly represent the opening phase of the eruption on 22 October as no tephra >1 cm in diameter was observed to have fallen >500 m from the vent after 23 October. We also took three lava samples whose times of eruption are unknown (Table 1), as well as one sample which was taken from an active pahoehoe toe and quenched in water (SN95-5; Table 1). A single sample of tephra from the 1979 eruption collected in 1991 (SN91-21) was analyzed with the 2005 samples for comparison.

Samples were imaged using a back-scattered electron detector on an SEM (Fig. 7). Glass from all tephra samples

Table 1 Major element compositions of glasses from Sierra Negra, determined by electron probe microanalysis

Sample	Eruption date	Material	SiO_2	TiO_2	Al_2O_3	FeO*	MnO	MgO	CaO	Na_2O	K_2O	P_2O_5	S	Total
SN-91-21	1979	Tephra	48.43	4.20	13.36	13.62	0.22	5.36	10.20	3.34	0.65	0.48	0.05	98.51
SN-05-01	27-Oct	Tephra	48.30	4.13	13.39	13.77	0.22	5.36	10.27	3.26	0.65	0.41	0.09	98.92
SN-05-02	22-Oct	Tephra	51.25	3.69	13.46	13.27	0.28	4.41	8.53	3.57	1.01	0.41	0.05	99.09
SN-05-04	28-Oct	Tephra	49.06	4.23	13.47	13.33	0.23	5.20	9.77	3.46	0.67	0.45	0.05	98.15
SN-05-06	28-Oct	Tephra	48.10	4.11	13.30	14.14	0.21	5.36	10.28	3.19	0.63	0.44	0.10	99.11
SN-05-07	29-Oct	Tephra	48.48	4.27	13.18	14.00	0.23	5.31	10.10	3.24	0.66	0.39	0.05	98.49
SN-05-08	Unknown	Lava	48.16	4.39	13.05	14.78	0.25	5.20	9.87	3.00	0.72	0.45	0.04	98.63
SN-05-11	29-Oct	Tephra	48.41	4.12	13.20	14.01	0.23	5.41	10.10	3.32	0.63	0.45	0.04	98.37
SN05-A	28-Oct	Tephra	51.03	3.70	13.47	13.14	0.21	4.44	8.71	3.80	0.95	0.47	0.03	98.64
SN-05 Hall	23-Oct	Tephra	48.78	4.12	13.35	13.65	0.25	5.20	10.03	3.34	0.69	0.58	0.01	98.32
SN-05-05	28-Oct	Lava	47.92	5.15	11.97	15.63	0.24	4.80	9.68	3.18	0.76	0.61	0.02	98.03
%RSD[a]			0.5%	1.5%	0.9%	3.5%	10.9%	1.1%	2.8%	5.1%	3.4%	21.9%	83.3%	

[a] % RSD is representative reproducibility based on six analyses of the same glass shard

and two lavas were analyzed by electron microprobe using the Cameca Camebax at Washington State University. A slightly defocused 15 kV, 15 nA beam was used, and sodium loss was monitored but negligible. Natural glass and mineral standards were used for calibration, and matrix effects corrected with a ZAF procedure. Representative estimates of precision were obtained via six replicate analyses of glass from each sample (Table 1). Plagioclase from tephra erupted on the first day and from the intracaldera lava flow were analyzed under the same conditions as glass.

Trace element analyses were carried out by inductively coupled plasma-mass spectrometer (ICP-MS) on an Agilent HP4500 at Colgate University according to methods described in Harpp et al. 2003). A suite of USGS standard reference materials was used as external standards (BIR-1, W-2, DNC-1, BHVO-2, AGV-2). Instrument drift was monitored using a 1:20 online dilution of an internal standard solution of ^{115}In and ^{133}Cs. Analyte masses were corrected to the nearest internal standard isotope. Replicate analyses of USGS standard W-2 were used to quantify accuracy and precision (Table 2).

Tephra sampled after the first day of the eruption is remarkably aphyric and glassy (Fig. 7). Most fragments of tephra only contain sparse microlites of plagioclase, with dimensions of <1×15 μm, and a few larger crystals ~5×30 μm. The average total crystal content in the 23–29 October tephra is 1.3%. Tephra erupted during the earliest phase of the eruption on 22 October has larger and more abundant microlites of plagioclase (Fig. 7b). The microlites are up to 10×100 μm in section and constitute 4.4% of the rock on average. Vesicles in all of the tephra range from >1 cm in diameter down to isolated bubble nuclei, which are as small as 2 μm.

The sample of pahoehoe that was collected and water-quenched as it oozed out of the sides of the caldera floor `a`a flow on 27 October (day 6) is notably more crystalline than any of the tephra. It contains 23% microlites of plagioclase and clinopyroxene (Fig. 7c). Plagioclase crystals have dimensions up to 20×120 μm, and clinopyroxene is up to 30×30 μm. The plagioclase in this rock ranges from An_{48} to An_{54} (Table 1).

Major element analyses of glass in tephra erupted after 23 October (day 2) and bulk-rock analyses of the lava samples are indistinguishable from those of the 1979 tephra, and among these samples there is no significant compositional variation (Figs. 8 and 9); we refer to this as the "main phase" of the eruption. The relative standard deviation (RSD) of the six tephra samples collected between 23 and 29 October is less than 3.5% for all the major elements, except for P_2O_5, for which the RSD is 15% and we attribute to greater analytical uncertainty (Table 1). In contrast, tephra erupted on the first day (SN05-2 and

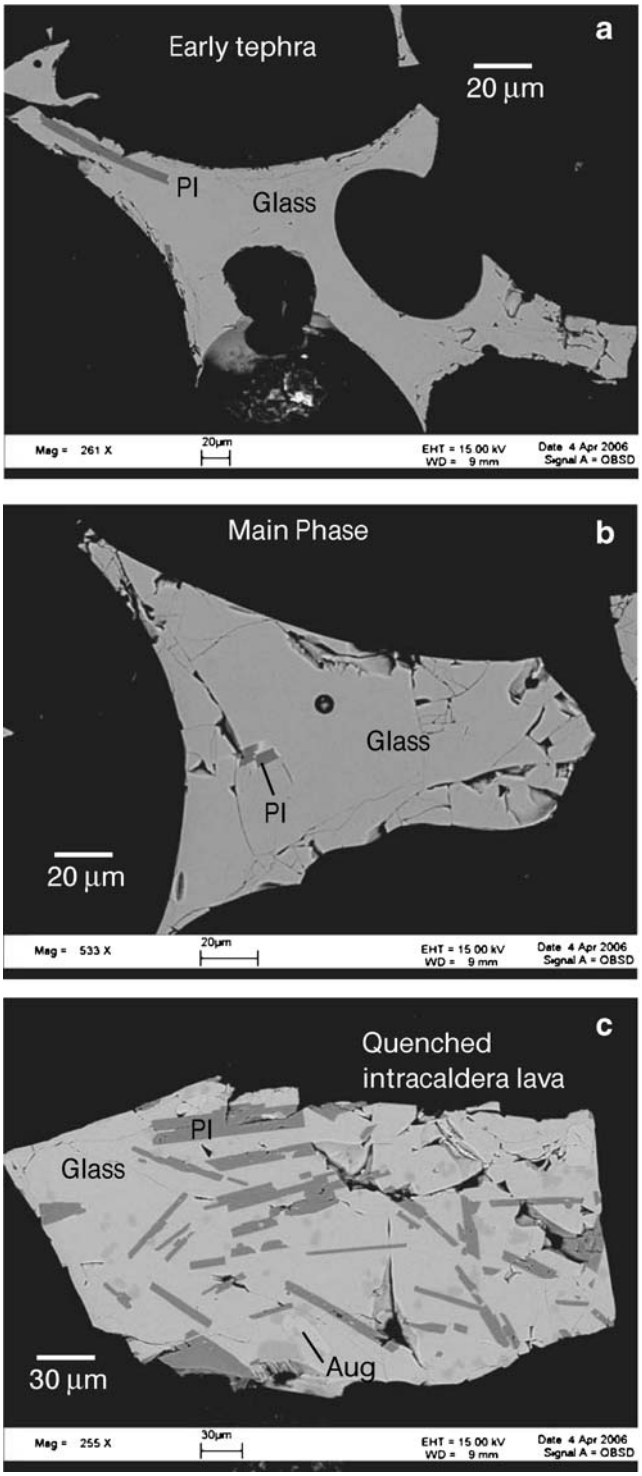

Fig. 7 Back-scattered electron images of tephra and lava from the 2005 eruption of Sierra Negra. *Top image* is SN05-2, from the initial phase of the eruption; *middle* is SN05-1 from the main phase (27 October), and *bottom* is sample taken and quenched from the intracaldera lava flow on 28 October. Plagioclase grains are *dark colored*, augite (*bottom image only*) is *light colored*, and glass is *medium gray*

Table 2 Trace element compositions of tephra and lava from Sierra Negra, determined by ICPMS

Sample	Eruption date	Material	Sc	V	Cr	Co	Ni	Cu	Zn	Rb	Sr	Y	Zr	Nb	Ba	La	Ce	Pr
SN-91-21	1979	Tephra	39.5	495	84	50	45	119	151	14	327	46	265	39.0	150.8	24.6	56.9	7.77
SN-05-01	27-Oct	Tephra	35.0	445	74	47	43	119	143	13	317	45	254	37.2	145.6	23.8	55.4	7.61
SN-05-02	22-Oct	Tephra	33.6	415	47	44	32	98	147	15	311	49	279	40.9	159.2	26.2	61.0	8.34
SN-05-04	28-Oct	Tephra	36.0	456	74	47	43	120	145	13	317	45	256	37.5	146.4	24.0	55.9	7.64
SN-05-06	28-Oct	Tephra	35.6	465	76	48	44	122	143	13	309	43	254	37.3	143.1	23.2	54.8	7.44
SN-05-07	29-Oct	Tephra	37.1	475	77	49	44	122	146	13	319	45	258	37.8	146.0	24.0	55.7	7.61
SN-05-08	Unknown	Lava	35.9	461	76	46	43	118	139	13	308	44	248	36.5	140.9	23.0	53.6	7.35
SN-05-11	29-Oct	Tephra	37.9	483	77	49	44	125	150	14	333	47	266	39.7	152.4	25.2	58.4	7.99
SN-05 Hall	23-Oct	Tephra	34.5	457	53	47	36	108	150	14	307	46	278	41.1	155.5	25.8	61.0	8.19
SN-05-05	28-Oct	Lava	37.3	467	80	48	45	123	146	13	323	46	259	38.1	146.3	23.9	55.8	7.66
SN-05-03	Unknown	Clastigenic lava	38.1	487	79	51	46	128	156	14	342	49	279	40.7	159.2	26.0	60.6	8.31
SN-05-09	Unknown	Lava	35.7	457	77	47	43	119	140	13	304	43	243	35.6	138.6	22.6	52.8	7.21
Precision %			3.8	3.6	3.8	3.3	3.3	2.8	2.0	4.5	2.0	1.7	2.0	1.8	0.9	2.5	2.1	1.3
			Nd	Sm	Eu	Gd	Tb	Dy	Ho	Er	Tm	Yb	Lu	Hf	Ta	Pb	Th	U
SN-91-21			33.8	8.47	2.76	8.91	1.43	8.25	1.66	4.44	0.63	3.73	0.537	6.09	2.41	2.15	2.15	0.62
SN-05-01			33.2	8.31	2.69	8.72	1.39	8.03	1.61	4.32	0.61	3.59	0.519	5.85	2.33	1.48	2.18	0.65
SN-05-02			36.2	9.03	2.89	9.39	1.50	8.66	1.74	4.66	0.65	3.90	0.562	6.30	2.53	1.80	2.41	0.74
SN-05-04			33.4	8.35	2.70	8.75	1.40	8.08	1.63	4.36	0.61	3.64	0.526	5.89	2.35	1.60	2.16	0.63
SN-05-06			32.5	8.17	2.65	8.50	1.36	7.89	1.59	4.24	0.60	3.56	0.506	5.81	2.32	1.44	2.05	0.62
SN-05-07			33.3	8.35	2.69	8.69	1.40	8.13	1.63	4.36	0.62	3.67	0.524	5.92	2.35	1.44	2.11	0.62
SN-05-08			32.1	8.03	2.63	8.44	1.36	7.81	1.57	4.25	0.59	3.54	0.508	5.68	2.27	1.39	2.03	0.61
SN-05-11			34.6	8.71	2.82	9.11	1.46	8.50	1.71	4.55	0.64	3.81	0.551	6.14	2.45	1.54	2.20	0.64
SN-05 Hall			35.4	8.97	2.84	9.20	1.47	8.48	1.71	4.56	0.64	3.79	0.549	6.35	2.54	1.77	2.20	0.67
SN-05-05			33.4	8.39	2.73	8.84	1.41	8.18	1.63	4.37	0.62	3.68	0.530	5.93	2.36	1.47	2.13	0.65
SN-05-03			36.1	9.03	2.94	9.44	1.51	8.73	1.76	4.71	0.66	3.97	0.570	6.39	2.53	1.57	2.38	0.71
SN-05-09			31.4	7.88	2.57	8.26	1.32	7.68	1.54	4.13	0.58	3.46	0.497	5.61	2.23	1.39	1.99	0.58
Precision %			1.3	1.9	1.4	1.5	1.5	2.0	1.8	1.4	2.0	1.4	1.9	1.5	1.6	1.5	1.9	4.1

Reported precision is representative reproducibility based on 14 analyses on the same solution of a standard rock

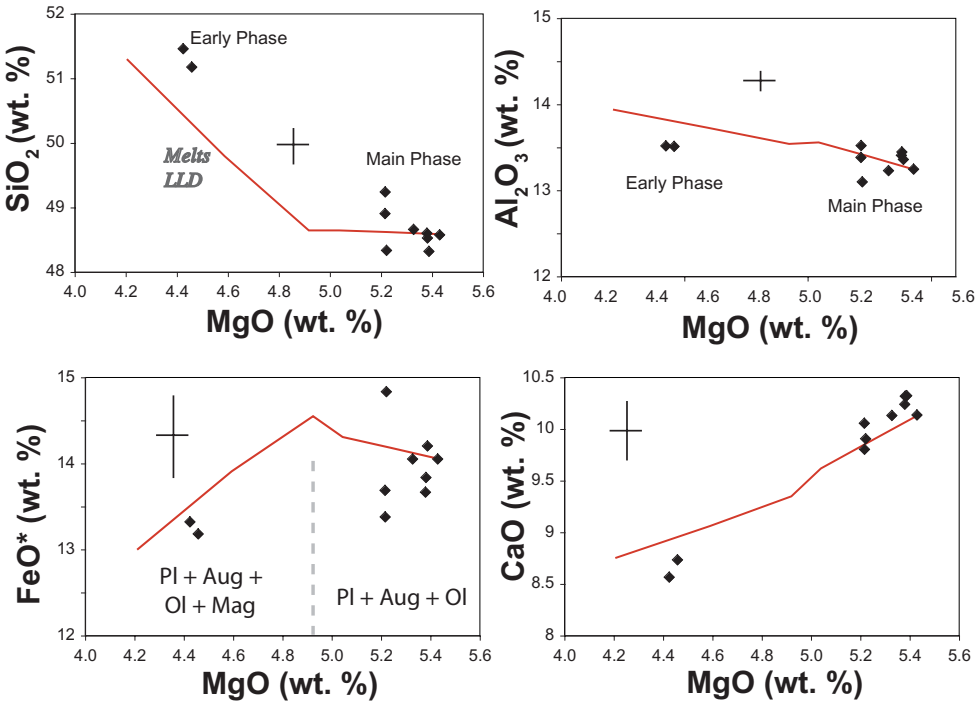

Fig. 8 Compositions of glasses from the 2005 eruption (data from Table 1) compared to model trends of MELTS for cooling from 1,128° to 1,108°C

SN05-A) is more evolved than main-phase tephra, (i.e., 4.41 wt% MgO, compared to 5.31 wt%; Figs. 8 and 9). Tephra from the first day also has lower CaO and TiO_2 abundances and higher K_2O.

Similar to the major elements, the trace elements define a narrow range of concentrations (Fig. 10), except for tephra produced on the first two days of the eruption. These earliest tephras have higher incompatible trace element contents than the average of the rest of the samples and exhibit lower Cr, Sc, and Ni, consistent with their evolved major element compositions.

Discussion

Changes in eruptive style

The style of the Sierra Negra 2005 eruption evolved through four stages:

1. An explosive vent-opening phase that produced an eruptive column ~13 km high
2. A curtain-of-fire phase, with lava fountains emanating from the ~2 km-long fissure
3. A focused-fountain phase, with continuously streaming gases propelling the fire fountains from isolated vents
4. A pulsing phase, with a periodically bursting lava fountain from a single vent

The changes in eruptive style can be related to current models of conduit flow and mechanisms of explosive basaltic eruptions, as discussed below.

Transition from curtain-of-fire to discrete vents

The ~2 km long fissure that characterized the beginning of the eruption focused to 2–3 vents by day 3, and to a single vent by day 4 or 5 before a second vent reopened. The vent focusing is consistent with observations from basaltic fissure eruptions of comparable size, as well as models of dike flow (e.g., Wolfe et al. 1988; Bruce and Huppert 1989; Wylie et al. 1999). Over the course of a few hours of flow within a dike, increases in temperature-dependent viscosity (Wylie et al. 1999) or partial solidification (Bruce and Huppert 1989) result in constriction of magma flow. Decreased mass flux leads to lower heat supply to constricted areas, resulting in a feedback mechanism that chokes much of the conduit but ultimately enlarges active

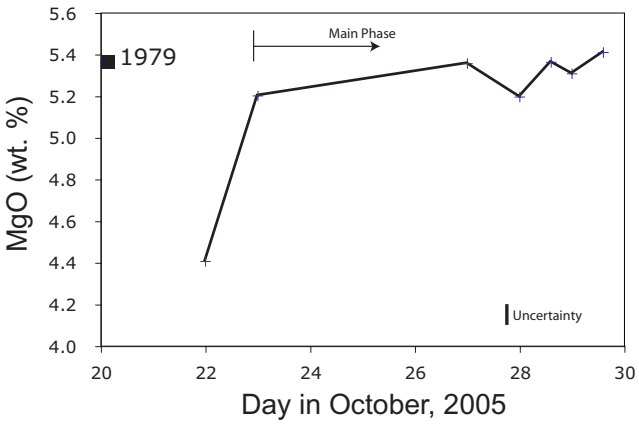

Fig. 9 Variation of MgO in tephra glasses over the course of the eruption. 1979 tephra is shown for comparison

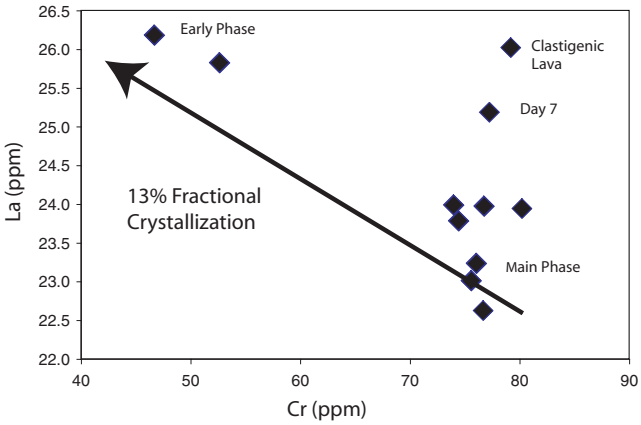

Fig. 10 Cr and La concentrations in samples of lava and tephra from throughout the eruption. Model arrow shows the effect of 13% fractional crystallization of an assemblage 48% augite, 40% plagioclase, and 12% magnetite, with mineral/melt distribution coefficients of 4, 0, and 30. Bulk distribution coefficient for La=0.01

vents and focuses eruptive activity to a few isolated locations along the original fissure. The transition from a continuous line of fountaining to several discrete vents, which coincided with a decrease in the net eruptive flux, is consistent with this explanation.

After the reopening of the easternmost vent on day 6, the intensity of the lava fountain at the continually active western vent was unaffected. This implies that the conduits supplying the two vents were isolated from each other by this stage of the eruption and were independently connected to the pressurized magma at depth, despite being only ~50 m apart at the surface.

Changes in lava fountain height

Head and Wilson (1987) propose that the height of a lava fountain depends most strongly on the magma's gas content and is relatively insensitive to the magma flux. The height of the lava fountains at the two main vents was nearly constant from day 3 through day 6 of the eruption, supporting Head and Wilson's (1987) hypothesis, because the generally decreasing eruptive flux and declining subsidence rate (Fig. 5) indicate that the pressure exerted by the magma chamber decreased throughout the eruption. The plume at the explosive beginning of the eruption and the progressively shrinking lava fountain on the last day are the exceptions to the constant lava-fountain height, suggesting that the initial magma was especially gas-rich, and decreased pressure of the chamber was important near the eruption's termination. Sierra Negra's lava-fountain height contrasts with observations from Pu'u 'O'o, (Kilauea, Hawaii) where Head and Wilson (1987) documented variations in fountain height within eruptive episodes, which they attributed to variable amounts of conduit degassing over the course of the eruption.

Using the relationships of Head and Wilson (1987), and given an estimated volume flux of 100 m^3 s^{-1} for the seventh day of the eruption and a fountain height of ~50 m, the exsolved magma volatile content was likely between 0.1 and 0.2 wt%. This range is valid for volume fluxes up to and exceeding 200 m^3 s^{-1}, and for fountain heights as small as 10–20 m, ranges that encompass most of the 2005 eruption. These estimates of the volume flux and magma gas content yield an estimate of the vent's diameter (Head and Wilson 1987) of 6–8 m. These calculations are complicated, however, by the presence of recycled pyroclasts or a lava pond within the vents (Parfitt et al. 1995), which reduce the velocity of the lava fountain. Thus, the above estimates of magmatic volatile contents and vent diameter are both probably minimums.

The Hawaiian to Strombolian transition

The 2005 Sierra Negra eruption underwent an important transition from Hawaiian to Strombolian style between days 7 and 8. Only the easternmost vent was active by this point, and its lava fountain ceased continuous jetting behavior and began pulsing. Large bursting bubbles were clearly visible in the pond at the base of the fountain. Bursts took place every 1–5 s, hurling pyroclasts up to 50 m into the air, the classic characteristic of Strombolian eruptions (e.g., Blackburn et al. 1976; Wilson 1980; Vergniolle and Brandeis 1996). During the Strombolian phase of the eruption, pyroclasts were too cold to contribute to a rootless flow, resulting in greater accumulation of scoriaceous tephra instead (e.g., Vergniolle and Mangan 2000).

The transition from Hawaiian to Strombolian styles has been attributed to a decrease in magma ascent speed below a certain threshold (Wilson 1980; Sparks 1978; Parfitt and Wilson 1995), and this explanation is consistent with the observations at Sierra Negra, where there was clearly a decrease in magma chamber pressure with time (Fig. 5). At relatively high ascent velocities, vesiculated magma moves through the conduit as a homogeneous two-phase flow (e.g., Wilson and Head 1981; Sparks 1978). As magma rise speed decreases, larger bubbles segregate and coalesce, forming a gas slug (e.g., Sparks 1978). Parfitt and Wilson (1995) estimate that the Hawaiian-Strombolian transition occurs when magma rise speeds are in the range of ~0.01–0.3 m s^{-1}. Rise speed can be estimated from observed volume flux divided by the estimated area of the eruptive vents (Parfitt 2004). Our estimates for volume flux for days 7 and 8 of the eruption, when the transition in eruptive behavior occurred, are 100 and 25 m^3 s^{-1}, and the vent diameter is calculated to be ~8 m. The magma rise rate for day 7 (Hawaiian style) is calculated to be 0.64 m s^{-1}; for day 8 (Strombolian), it drops to 0.32 m s^{-1}, broadly

consistent with the Hawaiian to Strombolian transition as calculated by Parfitt and Wilson (1995).

Clastigenic lava flows

The 2005 lava flows on the northern flank of Sierra Negra are all rootless clastigenic flows, fed by the lava fountains inside the caldera rim. Several factors led to the formation of these extensive flows. First, the low altitude wind during the eruption was mostly from the south, causing spatter and tephra to accumulate on the uppermost north flanks. Second, the easternmost vent produced an inclined fountain, directed to the north, so the pyroclasts accumulated disproportionately on that side of the vent. Third, the lava fountaining was vigorous, which allowed the pyroclasts to accumulate to lava-flow thickness before it cooled significantly (e.g., Capaccioni and Cuccoli 2005; Sumner et al. 2005).

During the curtain-of-fire phase, the clastigenic lava flows were active across a 2-km wide swath of the north flank, advancing ~5 km down the flank in <12 h. We estimate that the flows have an average thickness 4 m. These values yield estimates of the accumulation rate of pyroclasts of ~1,600 m/h, far beyond the minimum threshold for agglutination and welding (Capaccioni and Cuccoli 2005). The easternmost clastigenic flow, which remained active for a week, formed from pyroclasts averaging 1–5 cm in diameter. The accumulation rate of pyroclastic material must have exceeded 0.2 m h^{-1} over this week (Capaccioni and Cuccoli 2005). The deposition of up to 1 m of scoria on top of the easternmost clastigenic flow also contributed to its longevity, acting as insulation to slow cooling.

Ponded lava flow

The ponding of voluminous `a`a flows inside calderas is a common process in the Galápagos, and these lavas have distinctive characteristics that aid in the interpretation of the volcanoes' eruptive and structural histories. In addition to the 2005 eruption of Sierra Negra, ponded intracaldera lavas were emplaced during the 1982 eruption of Wolf volcano (Geist et al. 2005) and the 1960 eruption of Fernandina (Rowland and Munro 1992). Furthermore, many of the lavas described from the caldera walls at these volcanoes as well as Cerro Azul (Naumann and Geist 2000) and Ecuador (Geist et al. 2002) have been interpreted as having ponded in pre-existing calderas. Observation of the emplacement of the 2005 Sierra Negra lava revealed two unusual attributes, both related to the containment of the lava in a confined depression. First, the `a`a progressed by emitting a pahoehoe flow front, a process that has previously been recognized in Hawaii (Jurado-Chichay and Rowland 1995; Hon et al. 2003). Second, after the first day, the ponded lava flow grew in volume mostly through thickening by inflation, a process previously documented in the emplacement of pahoehoe lava flows (e.g., Hon et al. 1994; Self et al. 1998), but so far as we are aware, formerly unrecognized for `a`a flows. These unusual processes are attributed to the fact that the lava flow reached most of its maximum aerial extent within a day of the onset of the eruption, and thereafter its margins were contained within the inward-sloping caldera floor and walls.

The key element of inflationary pahoehoe is that once a surface crust forms to a sufficient thickness, it retards the flow top's horizontally advance. This permits a stable viscoelastic layer to form, which thickens as a function of the square root of time (Hon et al. 1994) and contains pressurized lava. Inflation is then driven by a pressure head in the fluid interior of the flow, which is in turn driven by gravity acting on lava contained inside the viscoelastic crust. During the first day of the 2005 eruption, the flow advanced as typical channel-fed `a`a. From the second day on, however, the crust of the ponded `a`a only advanced very slowly, perhaps a couple of meters per day, by slow spreading across elevated axial clefts (Fig. 11). We hypothesize that this transition in behavior occurred when a viscoelastic crust stabilized beneath the `a`a surface, between the brittle top and pressurized, near-Newtonian lava in the core of the flow (Hon et al. 1994; Self et al. 1998). The source of the internal pressure within the ponded `a`a was not derived from a sloping lava tube. Instead, lava cascaded down the bench in an open channel and pooled in a lava pond at the base of the escarpment. This elevated pool then supplied the interior of the lava flow, causing inflation and slow spreading.

This model (Fig. 11) also explains the effusion of the pahoehoe lobes from the interior of the `a`a flow and the extrusion of congealed toothpaste lava near the flow front. The effect of cooling within the intracaldera lava flow is modeled using MELTS, an energy-minimization model of crystallization of silicate liquids (Ghiorso and Sack 1995), using glass from the main phase tephra as a parent composition and setting the oxygen fugacity initially at Ni–NiO at the liquidus but closing the system to oxygen thereafter. The composition of the glass in quenched lava sample SN05-5 is best matched by 29°C of cooling, which results in the formation of 23% microlites. This small amount of cooling and crystallization almost certainly occurred while the lava was in the open channels on the caldera-wall benches, because thereafter it was contained entirely within the interior of the flow. When this still-hot and poorly crystalline lava broke out from the front margin of the stagnant `a`a flow, it acted as a low-effusion rate flow and created pahoehoe (Rowland and Walker 1990). In

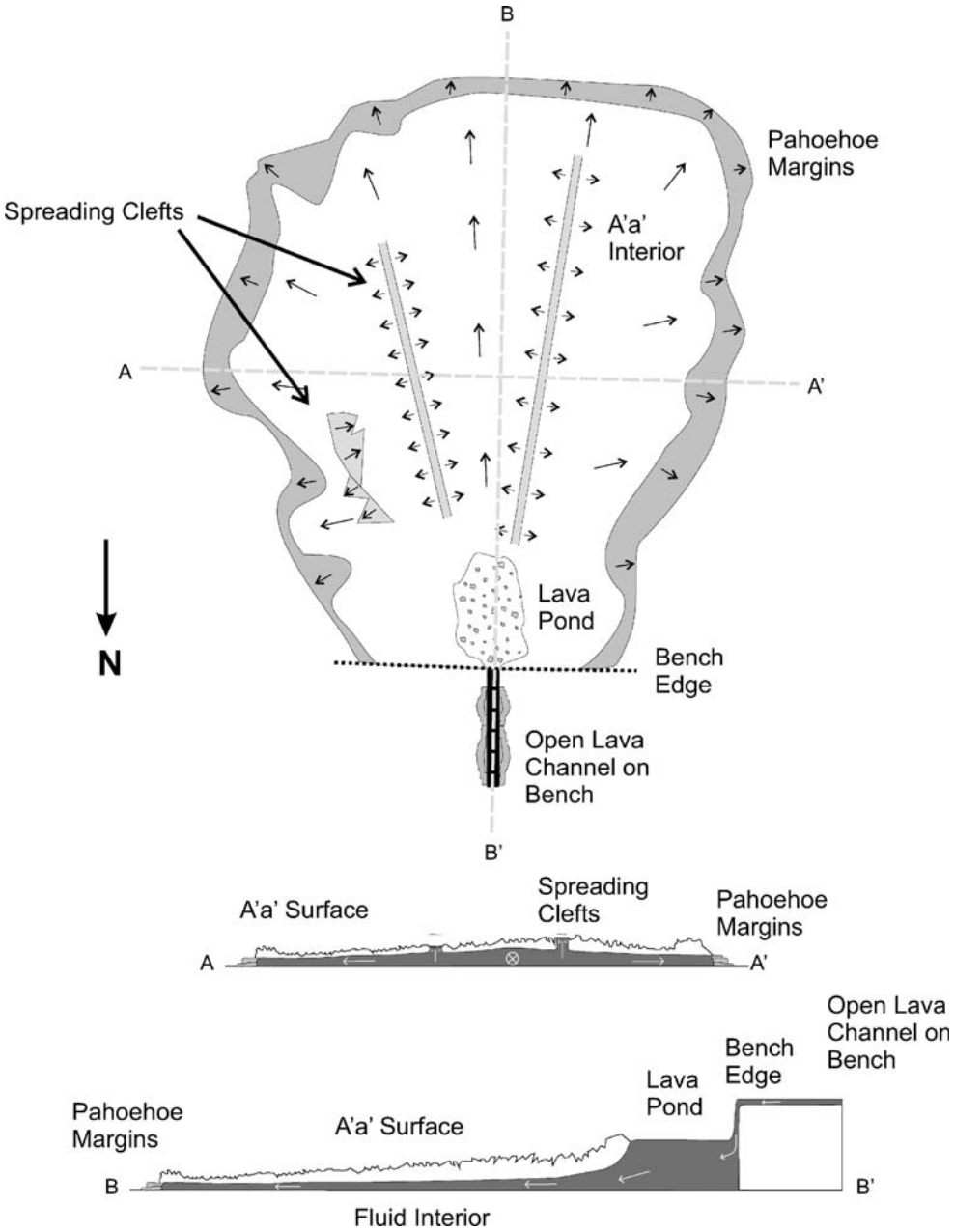

Fig. 11 Schematic diagram of the features in the caldera-filling lava flow (compare to Figs. 2 and 3). *Top*: plan view. *Middle*: cross section across the middle of the flow. *Bottom*: longitudinal cross section

places, the more slowly spreading `a`a would then advance over the pahoehoe front.

Volcano deformation

The absence of precursory changes in the deformation pattern (Figs. 4 and 5) indicates that the dike that fed the eruptive fissure likely started to propagate within the last 16 h before the eruption, after the GPS network failed. For example, if a dike that is 1 m wide at the surface had propagated from 2 to 1 km depth, GV03 should have moved ~7 cm southward (Pollard et al. 1983), and the absence of such observed motion indicates that this could not have happened, because the GV06-GV03 baseline shows no offset >5 mm from the long-term trend before 22 October. We suspect that the earthquake that preceded the eruption by ~3 h triggered the dike that fed the eruptive fissure. If so, then the dike ascended from the 2-km-deep magma chamber at a minimum velocity of 0.2 m s^{-1}.

Deflation during the eruption was caused by depressurization and loss of magma from the subcaldera magma reservoir. Moreover, intrusion of the dike and opening of the eruptive fissure contributed to deformation. Modeling of the deformation is severely hampered by the absence of any stable GPS station in the region for the first three days of the eruption and the lack of coherence within the caldera in co-eruption interferograms. Thus, we have made best estimates of most parameters before inverting for

unknowns. The four GPS stations operating over the course of the eruption do not constrain the geometry of the magma body well, but the long-term deformation at Sierra Negra indicates a flat-roofed chamber (perhaps a sill), roughly 5×3 km in horizontal extent, and whose top is about 2.1 km deep (Amelung et al. 2000; Geist et al. 2006; Yun et al. 2006a). The minimum subsidence of GV04 was 2.4 m over the course of the eruption (with the most conservative assumption that GV03 underwent no subsidence). A more realistic estimate, arrived at by extrapolating the long-term uplift of GV03 to 22 October and comparing that to its position on 24 October (when its position relative to a stable station could be determined), is that the total subsidence at GV04 was 5.4 m. The minimum subsidence requires that the chamber contracted in volume by 8.3×10^7 m^3, using the geometry modeled by Geist et al. (2006) and the method of Okada (Okada 1985). The more realistic estimate of subsidence yields an estimated contraction of the magma chamber of 1.9×10^8 m^3. This calculated range in eruptive volume from deformation data is consistent with our maximum volume estimate of 1.5×10^8 m^3.

We also modeled the most coherent radar interferogram (Fig. 6a) to gain insight into the magma source associated with the eruption. Unfortunately, deformation due to the intrusion of the dike along the north caldera rim cannot be resolved because of the lack of coherent data within the caldera We first modeled the InSAR data by assuming a uniformly closing, horizontal dislocation at 2.1 km depth (Amelung et al. 2000; Geist et al. 2006; Yun et al. 2006a, b) and solved for aerial extent and opening (Okada 1985). The best-fitting dislocation to the co-eruption interferogram is slightly larger in plan view than that of Geist et al. (2006), reaching a size of about 5×5 km centered within the caldera, with a volume loss of 66×10^6 m^3. The maximum expected subsidence in the caldera from this model is less than 2 m, a smaller value than the minimum estimated GPS displacement. We note that these estimates are poorly constrained, owing to the lack of coherence where it is most needed for modeling.

A point source model is required to explain the line-of-sight shortening east of the caldera, so we combined a point source and a sill source to best approximate the deformation field. The best-fitting model has a 4.5×4.5 km uniform opening sill and a point source, and both located at 2.1 km depth beneath the caldera (Fig. 6b). The cumulative volume loss from the two model sources is 80×10^6 m^3, and the maximum predicted subsidence within the caldera is about 3.5 m, which are within the range of estimates from the GPS measurements. The residual displacements (Fig. 6c) are significant in some areas, especially the south and east parts of the caldera, because of the lack of data in the caldera where deformation gradients are highest. Refinements to the deformation models are currently being under taken by Sang-Ho Yun and his colleagues at Stanford University, who have developed methods to obtain meaningful InSAR measurements within the caldera (Yun et al. 2006b).

The deformation of Sierra Negra is coupled closely in time to the eruptive flux. The subsidence rate decelerated exponentially over the course of the eruption (Fig. 5). The eruptive flux is poorly constrained, because we have no way of knowing if the depths of the lava channels changed over the course of the eruption. If, however, we use the cumulative width of the lava channels spilling over the caldera bench (measured in photographs taken during the course of the eruption) as a proxy for flux, there is a direct correlation between flux and deformation rate (Fig. 12), indicating nearly immediate elastic response of the caldera floor to the eruption of magma.

Petrologic interpretation

The range of glass compositions (Fig. 6) cannot simply be the result of in situ microlite crystallization, because the tephra contains <5% crystals, which is not enough to account for the variation (Fig. 7). Also, bulk-rock (glass + crystals) trace element compositions display significant variation (Fig. 10). Relative to the main-phase tephra and lavas, the first tephra erupted is enriched in incompatible elements by >10% and depleted in elements compatible in plagioclase, clinopyroxene, and magnetite (Table 1, Fig. 10). The difference in trace element composition between the first-erupted and main-phase tephra is reproduced by ~13% crystallization (Fig. 10). The compositions of the rocks show strong evidence for crystallization of both plagioclase (lower Sr/Y) and clinopyroxene (lower Sc/Y) crystallization in the first-erupted lavas (Fig. 13).

The major element evolution of the Sierra Negra magma within the subcaldera reservoir is modeled using MELTS (Ghiorso and Sack 1995) at 70 MPa, because the top of the magma chamber at Sierra Negra is known to be about 2.1 km deep (Amelung et al. 2000; Geist et al. 2006). The oxygen fugacity was initially set at Ni–NiO at the liquidus, but the system was closed to oxygen upon cooling. The initial water concentration was set at 0.6%. The model shows that the entire range in glass compositions is likely due to crystallization of plagioclase, olivine, augite, and titanomagnetite, by cooling from 1,128 to 1,108°C (Fig. 8).

Two explanations for the intra-eruption zoning and the differentiation of the early-phase magma are possible. First, the initial magma that intruded through the conduit may have cooled and undergone fractional crystallization as it ascended. Second, the early-phase magma may have erupted from a differentiated upper boundary layer in the subcaldera magma body.

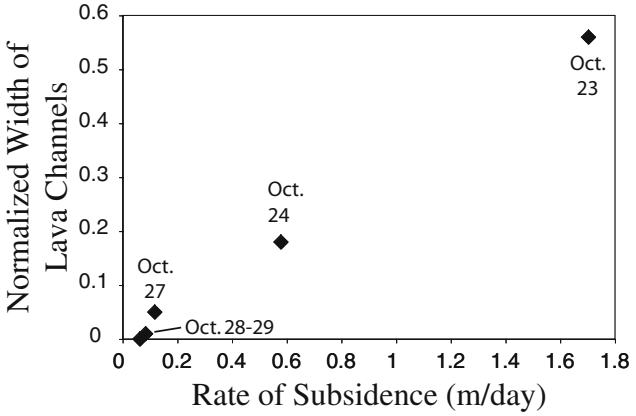

Fig. 12 Subsidence of the caldera correlates almost perfectly with the eruptive flux. Horizontal axis is the rate of subsidence of GPS station GV04 relative to GV03, which decelerated over the course of the eruption. Vertical axis is the proportion of the caldera bench edge that is covered by an open lava channel, which is proportional to the eruptive flux, if the depth of the channels is the same

The complete absence of crystals >100 μm in the early phase tephra argues against crystallization and removal of the crystals during ascent. The lack of a deformation signal in the days prior to the eruption also suggests that the dike that fed the eruptive fissure intruded only hours before the eruption, perhaps initiated by the earthquake that occurred earlier on 22 October. Nucleation, growth, and near-perfect removal of >10% crystals in the matter of a few hours is implausible. Cashman (1993) estimated that plagioclase growth rates are in the range of 10^{-10} to 10^{-11} cm s^{-1} in shallow basaltic dikes. Thus growth of the 100 μm microlites observed in the rock would have taken weeks to years. In addition to crystal growth and nucleation, both preexisting and newly formed crystals need to be perfectly segregated from the liquid during ascent through the fissure-feeding dike, which is estimated to have propagated at ~0.2 m s^{-1}.

We therefore suggest that the magma body that lies 2.1 km beneath the caldera is stably zoned, with an upper thermal boundary layer that is cooler and more evolved than the interior of the magma body. According to results from MELTs calculations, the first 20° of cooling causes approximately 13% crystallization of plagioclase, clinopyroxene, olivine and titanomagnetite. Because the residual liquid is slightly buoyant relative to the undifferentiated magma (the calculated density is 2,670 versus 2,700 kg/m^3) and crystals, it is unlikely that the differentiated liquid could have been created in an upper solidification front (Marsh 1996, 2002). In contrast, Helz et al. (1989) found that buoyant differentiated liquid pooled in the upper part of the Kilauea Iki lava lake. This liquid derived from the lower solidification front and is hypothesized to have risen to the top of the magma body in buoyant diapirs, with no mixing. Jellinek and Kerr (Jellinek and Kerr 2001) have argued against this hypothesis but their model invokes vigorous convection in the lava lake an unresolved issue. In the Helz et al. (1989) model diapirs are driven by a density contrast of ~20 kg/m^3 nearly that calculated for the Sierra Negra chamber.

Thus, our preferred explanation is that a pool of differentiated liquid accumulated beneath the upper solidification front of the Sierra Negra magma chamber. This differentiated liquid formed from ~13% crystallization near the bottom of the reservoir, and the liquid rose buoyantly through the main body. Additional crystallization of microlites without crystal-liquid segregation then took place with ~5° further cooling in the upper boundary layer and during conduit ascent. As the shallow magma body at Sierra Negra became increasingly pressurized by intrusion, the surrounding rocks eventually failed, and the first magma erupted was from this mostly liquid-differentiated upper-boundary layer. The differentiated magma was evacuated in the first hours of the eruption, and later products are from the relatively homogeneous interior of the magma body. One of the attractive aspects of this model is that crystallization would also tend to enrich the differentiated melt in water, which accounts for the greater explosivity of the first phase of the eruption.

The nearly aphyric rocks erupted during October 2005 at Sierra Negra provide almost no evidence regarding the composition of the parental magma that intruded and pressurized the reservoir. We suspect that it is evolved basalt, not much different from what was erupted during the main phase, because exposed Sierra Negra lavas are remarkably homogeneous in composition and contain no evidence of xenocrysts derived by crystallization of a more primitive magma (Reynolds and Geist 1995).

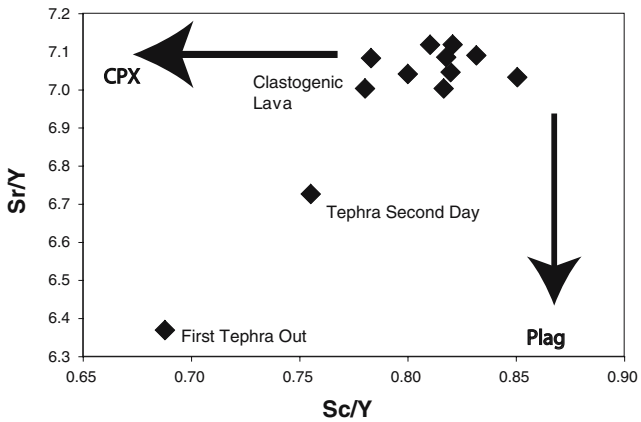

Fig. 13 Plot of Sc/Y versus Sr/Y for 2005 tephra and lava. The early phase tephra has lower Sr/Y and Sc/Y than the main phase rocks, indicating an origin by fractionation of both plagioclase and pyroxene

Conclusion: a bottom-up view of the 2005 eruption

This study reveals that even in a remote setting with little instrumentation, an integrated study of an active eruption can reveal much about eruptive processes and the dynamics of magma transport. Deformation data indicate that the magma chamber feeding summit eruptions at Sierra Negra is a sill or flat-topped diapir that lies 2.1 km beneath the caldera floor (Amelung et al. 2000; Geist et al. 2006; Yun et al. 2006a). This reservoir is pressurized by magma intruding from below, which is already differentiated. Cooling takes place at the roof and floor of the magma body; residual liquids at the roof do not segregate from the crystals, but residual liquids formed at the floor are buoyant and segregate to the roof of the reservoir after about 13% crystallization. This differentiated magma is about 20°C cooler than the main body and is relatively rich in dissolved H_2O.

The subcaldera magma reservoir has been intruded episodically since at least 1992 (Amelung et al. 2000) and probably since the previous eruption in 1979. These events pressurized the sill, which domed the caldera floor by >5 m and caused repeated inelastic failure along trapdoor faults (Chadwick et al. 2006). Although the pressure increase accelerated starting in 2003, there is no indication of any sudden change in the days leading up to the eruption.

At 14:34 local time on 22 October 2005, a M_w 5.5 earthquake occurred at Sierra Negra. This earthquake probably initiated dike injection from the magma reservoir, but the dike did not propagate along the active fault: instead, it followed a path on the side of the volcano *opposite* the active faults. That the dike avoided the active faults is consistent with the long-term mechanical and recent eruptive behavior of Sierra Negra (Reynolds et al. 1995; Yun et al. 2006a).

The first magma that erupted was chemically more evolved and richer in water than the magma that erupted later. Its eruption led to the formation of a ~13 km high plume of steam, gases, and ash. Within an hour, the dike was delineated by a 2-km-long curtain of fire. The fountains fed clastigenic flows that quickly progressed down the north side of the volcano. They also supplied a voluminous `a`a flow that advanced 5 km south across the caldera floor, banked against the southern caldera wall, and then flowed west in the moat between the trapdoor fault and caldera wall. The intra-caldera lava flow grew to most of its final area within the first two days of the eruption. The rootless clastigenic flows formed because the deposition rate of the tephra and spatter on the uppermost north flank was rapid, maintained by high effusion rates at the start of the eruption, a favorable wind direction, and collimated lava fountains later in the eruption.

The curtain-of-fire phase ended when the fissure focused into several vents at its eastern end, probably owing to constriction of the dike from cooling, increases in viscosity, and a focusing feedback mechanism (Wylie et al. 1999). All but the easternmost rootless flow ceased activity once the vents coalesced from the fissure. Except for the opening blast, this phase of eruptive activity was Hawaiian in style, with continuously streaming gases carrying spatter and tephra in the fire fountain.

Lava continued to pond within the caldera after flowing over intracaldera benches in open channels. The caldera floor lava flow was fed by a perched lava pond beneath the bench, which fed the interior of the main flow and pressurized it, causing slow inflation and slight spreading about its center. After the first day, the `a`a flow advanced slowly by emitting lobes of pahoehoe.

On the last day of the eruption, the eruptive style changed to Strombolian, characterized by the bursting of large bubbles near the surface and pulsating fire fountains. The transition occurred when the ascent rate of the magma in the conduit decreased below a threshold value of ~25 m^3 s^{-1}, probably owing to waning driving pressure from the magma chamber. The eruption ended in the early hours of 30 October 2005, when the cooling rate within the dike exceeded a critical flow rate, a reflection of continually decreasing driving pressure. The magma reservoir began inflating the next day.

Acknowledgements We would like to extend our thanks to the Galápagos National Park and the Charles Darwin Research Station, who made our observation of the Sierra Negra eruption possible, particularly Srs. O. Carvajal, W. Tapia, F. Cruz, and G. Watkins. We are also grateful to individuals who have provided us with images from the early phases of the eruption, including G. Estes, F. Cruz, and A. Voigt. Thanks to J. Normandeau of UNAVCO for his heroic patience in helping us get the GPS receivers working again during the eruption. This work was supported by NSF grants EAR-0207425 to KSH and EAR-0207605, 0538205, and 0004067 (which supported the installation of the GPS network) to DJG. ENVISAT ASAR data are copyrighted 2004–2006 by the European Space Agency, and were obtained via Category-1 Proposal 3493. Thanks to W. Tater for his help with the SEM. We thank B. Cousens and especially S. Rowland for review and J. Stix for his editorial help.

References

Allan JF, Simkin R (2000) Fernandina Volcano's evolved, well-mixed basalts: mineralogical and petrological constraints on the nature of the Galapagos plume. J Geophys Res 105:6017–6031

Amelung F, Jonsson S, Zebker H, Segall P (2000) Widespread uplift and 'trapdoor' faulting on Galapagos volcanoes observed with radar interferometry. Nature 407:993–996

Blackburn EA, Wilson L, Sparks RSJ (1976) Mechanisms and dynamics of Strombolian activity. J Geol Soc London 132:429–440

Bruce PM, Huppert HE (1989) Thermal control of basaltic fissure eruptions. Nature 342:665–667

Capaccioni B, Cuccoli F (2005) Spatter and welded air fall deposits generated by fire-fountaining eruptions: cooling of pyroclasts

during transport and deposition. J Volcanol Geotherm Res 145:263–280
Cashman KV (1993) Relationship between plagioclase crystallization and cooling rate in basaltic melts. Contrib Mineral Petrol 113:126–142
Chadwick WW, Geist DJ, Johnsson S, Poland M, Johnson DJ (2006) A volcano bursting at the seams: inflation, faulting, and eruption at Sierra Negra Volcano, Galápagos. Geology 34:1025–1028
Geist D (2002) Volcanic evolution in the Galapagos: the dissected shield of Volcan Ecuador. Geochem Geophys Geosyst 3(10): 1061. DOI 10.1019/2002GC000355
Geist DJ, Naumann TR, Standish JJ, Kurz MD, Harpp KS, White WM, Fornari DJ (2005) Wolf Volcano, Galapagos Archipelago: melting and magmatic evolution at the margins of a mantle plume. J Petrol 46:2197–2224
Geist D, Chadwick W, Johnson D (2006) Results from new GPS and gravity monitoring networks at Fernandina and Sierra Negra volcanoes, Galapagos, 2000–2002. J Volcanol Geotherm Res 150:79–97
Ghiorso MS, Sack RO (1995) Chemical mass transfer in magmatic processes: IV. a revised and internally consistent thermodynamic model for the interpolation and extrapolation of liquid-solid equilibria in magmatic systems at elevated temperatures and pressures. Contrib Mineral Petrol 119:197–212
Goff F, McMurtry GM, Counce D, Simac JA, Roldan-Manzo AR, Hilton DR (2000) Contrasting hydrothermal activity at Sierra Negra and Alcedo volcanoes, Galapagos Archipelago, Ecuador. Bull Volcanol 62:34–52
Harpp KS, Fornari DJ, Geist DJ, Kurz MD (2003) Genovesa Submarine Ridge: a manifestation of plume-ridge interaction in the Northern Galápagos Islands. Geochem Geophys Geosys 4 DOI 10.1029/2003GC000531
Head JW, Wilson L (1987) Lava fountain heights at Pu'u O'o, Kilauea, Hawaii: indictators of amount and variations of exsolved magma volatiles. J Geophys Res 92:13,715–713,719
Helz RT, Kirschenbaum H, Marinenko JW (1989) Diapiric transfer of melt in Kilauea Iki lava lake, Hawaii: a quick, efficient process of igneous differentiation. Geol Soc Am Bull 101:578–594
Hon KA, Gansecki C, Kauahikaua J (2003) The transition from 'a'a to pahoehoe crust on flows emplaced during the Pu'u 'O'o-Kupaianaha eruption. US Geol Surv Prof Pap 89-103
Hon K, Kauahikaua J, Denlinger R, Mackay K (1994) Emplacement and inflation of pahoehoe sheet flows: observations and measurements of active lava flows on Kilauea volcano, Hawaii. Geol Soc Am Bull 106:351–370
Jellinek AM, Kerr RC (2001) Magma dynamics, crystallization, and chemical differentiation of the 1959 Kilauea Iki lava lake, Hawaii, revisited. J Volcanol Geotherm Res 110:235–263
Jonsson S, Zebker H, Amelung F (2005) On trapdoor faulting at Sierra Negra volcano, Galapagos. J Volcanol Geotherm Res 144:59–71
Jurado-Chichay Z, Rowland SK (1995) Channel overflows of the Phue Bay flow, Mauna Loa, Hawai'i: examples of the contrast between surface and interior lava. Bull Volcanol 57(2):117–126
Marsh BD (1996) Solidification fronts and magmatic evolution. Mineral Mag 60:5–40
Marsh BD (2002) On bimodal differentiation by solidification front instability in basaltic magmas, part 1: basic mechanics. Geochim Cosmochim Acta 66:2211–2229
Naumann TR, Geist D (2000) Physical volcanology and structural development of Cerro Azul Volcano, Isabela Island, Galapagos: implications for the development of Galapagos-type shield volcanoes. Bull Volcanol 61:497–514
Okada Y (1985) Surface deformation due to shear and tensile faults in a half-space. Bull Seism Soc Am 75:1135–1154
Parfitt EA (2004) A discussion of the mechanisms of explosive basaltic eruptions. J Volcanol Geotherm Res 134:77–107
Parfitt EA, Wilson L (1995) Explosive volcanic eruptions: IX. the transition between Hawaiian-style lava fountaining and Strombolian explosive activity. Geophys J Int 121:226–232
Parfitt EA, Wilson L, Neal CA (1995) Factors influencing the height of Hawaiian lava fountains: implications for the use of fountain height as an indicator of magma gas content. Bull Volcanol 57:440–450
Pollard DD, Delaney PT, Duffield WA, Endo ET, Okamura AT (1983) Surface deformation in volcanic rift zones. Tectonophys 94:541–584
Rader E, Harpp KS, Geist DJ (2006) Eruption dynamics and flow morphology during the 2005 Sierra Negra eruption, Galapagos Islands. EOS Trans AGU Fall Meet Assem Suppl 87:Abstract V23A-0586
Reynolds RW, Geist DJ (1995) Petrology of lavas from Sierra Negra volcano, Isabela Island, Galapagos Archipelago. J Geophys Res 100:24,537–524,553
Reynolds RW, Geist D, Kurz MD (1995) Physical volcanology and structural development of Sierra Negra volcano, Isabela Island, Galapagos Archipelago. Geol Soc Am Bull 107:1398–1410
Rowland SK, Walker GPL (1990) Pahoehoe and aa in Hawaii: volumetric flow rate controls the lava structure. Bull Volcanol 52 (8):615–628
Rowland SK, Munro D (1992) The caldera of Volcan Fernandina: a remote sensing study of its structure and recent activity. Bull Volcanol 55:97–109
Self S, Keszthelyi L, Thordarson T (1998) The importance of pahoehoe. Ann Rev Earth Planet Sci 26:81–110
Simkin T, Siebert L (1994) Volcanoes of the world. Geoscience Press, Tucson, AZ
Sparks RSJ (1978) The dynamics of bubble formation and growth in magmas: a review and analysis. J Volcanol Geotherm Res 3:1–37
Sumner JM, Blake S, Matela RJ, Wolff JA (2005) Spatter. J Volcanol Geotherm Res 142:49–65
Teasdale R, Geist D, Kurz M, Harpp K (2005) 1998 eruption at Volcan Cerro Azul, Galapagos Islands: I. syn-eruptive petrogenesis. Bull Volcanol 67:170–185
Vergniolle S, Brandeis G (1996) Strombolian explosions 1: a large bubble breaking at the surface of a lava column as a source of sound. J Geophys Res 101:20,433–420,447
Vergniolle S, Mangan MT (2000) Hawaiian and Strombolian eruptions. In: Sigurdsson H, Houghton B, McNutt SR, Rymer H, Stix J (eds) Encyclopedia of volcanoes. Academic Press, San Diego, CA, pp 447–461
Wilson L (1980) Relationships between pressure, volatile content and ejecta velocity in three types of volcanic explosion. J Volcanol Geotherm Res 8:297–313
Wilson L, Head JW (1981) Ascent and eruption of basaltic magma on the Earth and Moon. J Geophys Res 86:2971–3001
Wolfe EW, Neal CA, Banks NG, Duggan TJ (1988) Geologic observations and chronology of eruptive events. US Geol Surv Prof Pap 1463:1–97
Wylie JJ, Helfrich KR, Dade B, Lister JR, Salzig JF (1999) Flow localization in fissure eruptions. Bull Volcanol 60:432–440
Yun S, Zebker H, Segall P, Hooper A, Poland M (2005) The 2005 eruption at Sierra Negra volcano unveiled by InSAR observations, EOS Trans AGU Fall Meet Assem Suppl 87(52):Abstract G52A-01
Yun S, Segall P, Zebker H (2006a) Constraints on magma chamber geometry at Sierra Negra Volcano, Galapagos Islands, based on InSAR observations. J Volcanol Geotherm Res 150:232–243
Yun S, Zebker H, Segall P, Hooper A, Poland M (2006b) 2005 Eruption at Sierra Negra volcano unveiled by InSAR observations. EOS Trans AGU Fall Meet Assem Suppl 87(52):Abstract G52A-01